PNAS RESEARCH ARTICLE | CHEMISTRY BIOCHEMISTRY

A new capacity of gut microbiota: Fermentation of engineered inorganic carbon nanomaterials into endogenous organic metabolites

Xuejing Cui[a,b], Xiaoyu Wang[a,c], Xueling Chang[d], Lin Bao[a,c], Junguang Wu[a,c], Zhiqiang Tan[e], Jinmei Chen[f], Jiayang Li[a], Xingfa Gao[a], Pu Chun Ke[b], and Chunying Chen[a,b,c,1]

Edited by Catherine Murphy, University of Illinois at Urbana-Champaign, Urbana, IL; received November 3, 2022; accepted April 16, 2023

Carbon-based nanomaterials (CNMs) have recently been found in humans raising a great concern over their adverse roles in the hosts. However, our knowledge of the in vivo behavior and fate of CNMs, especially their biological processes elicited by the gut microbiota, remains poor. Here, we uncovered the integration of CNMs (single-walled carbon nanotubes and graphene oxide) into the endogenous carbon flow through degradation and fermentation, mediated by the gut microbiota of mice using isotope tracing and gene sequencing. As a newly available carbon source for the gut microbiota, microbial fermentation leads to the incorporation of inorganic carbon from the CNMs into organic butyrate through the pyruvate pathway. Furthermore, the butyrate-producing bacteria are identified to show a preference for the CNMs as their favorable source, and excessive butyrate derived from microbial CNMs fermentation further impacts on the function (proliferation and differentiation) of intestinal stem cells in mouse and intestinal organoid models. Collectively, our results unlock the unknown fermentation processes of CNMs in the gut of hosts and underscore an urgent need for assessing the transformation of CNMs and their health risk via the gut-centric physiological and anatomical pathways.

carbon nanomaterials | gut microbiota | fermentation | organic butyrate | intestinal stem cells

Due to their distinct and diverse properties, carbon-based nanomaterials (CNMs) have been applied in various fields including consumer products, biomedicine, and industry (1–3). Considerable evidence has demonstrated the presence of CNMs in various food items (beverages, roast meat, and hamburgers) (4, 5), environmental media (6–8), and clinically approved oral CNMs drug (graphene-like structure) (2). Especially, carbon nanotubes have been found in the bronchoalveolar lavage fluid in 69 Parisian children (9, 10) and human oral cavity (11, 12). Oral ingestion occurs consequentially to swallowing inhaled nanomaterials following mucociliary clearance or direct food/drinking/drug ingestion. Obviously, the human gut exposure to these nanoparticles through oral route is inevitable, which has become a very realistic problem and a great concern (13). Although some studies have implicated the direct adverse effects of CNMs on living organisms (14–18), the fundamental behavior and processes of CNMs in biological hosts including their degradation, transformation, and bioavailability are not understood. This lack of understanding prevents an accurate evaluation of the toxicity of CNMs in organisms.

The human gut hosts a complex ecosystem of microbes that play pivotal roles in metabolism, food digestion and clearance of invading particles/pathogens, and active nutritive connection with other body organs, thus determining the human health (19, 20). After CNMs enter the intestine, trillions of microbes act as both their first barrier and their primary targets (2, 21, 22). As a "forgotten organ," the gut microbiota exerts the functions of extracting and fermenting carbon compounds from dietary fibers for metabolite synthesis (23). The elemental carbon is the structural unit of most metabolites and is essential to regulate all activities in whole life of organism. Given the observed degradability of CNMs/polymers in artificial enzymatic systems (24–28), eukaryotic systems (29), and environmental aerobic microbes (30–34), we postulated that gut microbiota (99% obligate anaerobes) may be capable of exploiting CNMs and the inorganic carbon derived from CNMs may induce unique biological processes impacting their biotransformation and bioavailability and, furthermore, fate in the gut. Several central questions underlying the behavior of CNMs remain: i) Can the gut microbiota ferment CNMs just like dietary fibers and can the inorganic carbon of CNMs be transformed into organic metabolites? ii) Which specific pathway and gut bacteria participate in CNMs fermentation? iii) What are the biological consequences of the CNMs transformation?

Significance

Gut microbiota-governed biological processes determine the final fate and adverse outcomes of CNMs in the gut of hosts. Consequently, addressing the knowledge gaps regarding the gut microbiota-mediated biological processes/behaviors and harmful effects of CNMs is critical. We revealed that exogeneous inorganic CNMs underwent fermentation processes and were fermented as a bioavailable source into organic butyrate (biologically functional molecule) by gut microbiota. In particular, the interactive metabolite (butyrate) of CNMs and gut bacteria inhibited the function of neighboring intestinal stem cells. This work provides evidence on the incorporation of CNMs into metabolic carbon flow in gut microbiota for the production of short-chain fatty acids, which influences the effects of CNMs on the gut homeostasis.

Author contributions: X. Cui and C.C. designed research; X. Cui, X.W., L.B., J.W., Z.T., and J.C. performed research; X. Cui, X. Chang, L.B., J.L., and X.G. contributed new reagents/analytic tools; X. Cui, X.G., and C.C. analyzed data; and X. Cui and C.C. wrote the paper.

The authors declare no competing interest.

This article is a PNAS Direct Submission.

[1]To whom correspondence may be addressed. Email: chenchy@nanoctr.cn.

This article contains supporting information online at https://www.pnas.org/lookup/suppl/doi:10.1073/pnas.2218739120/-/DCSupplemental.

Published May 8, 2023.

To fill this knowledge gap, two most representative CNMs, one-dimensional single-walled carbon nanotubes (SWCNTs) and two-dimensional graphene oxide (GO) nanosheets, were used. We revealed that the gut microbiota effectively converted exogenous CNMs and microbial metabolism was responsible for this action. After a comprehensive investigation of the transformation–fermentation processes of CNMs in vitro and in vivo using isotope labeling and tracing techniques, we demonstrated that CNMs were fermented as a special carbon source and the inorganic carbon from CNMs was eventually incorporated by butyrate-producing bacteria, the dominant bacteria which exploited the CNMs into butyrate through the pyruvate pathway, further affecting the function of intestinal stem cells and beyond.

Results and Discussion

Gut Microbiota Ferments Inorganic Carbon Nanomaterials into Organic Metabolites. The well-established protocols with modifications were used to prepare oxidized SWCNTs and GO (35). The size, morphology, and oxidation status of the SWCNTs and GO were carefully characterized and presented in *SI Appendix*, Fig. S1. Transmission electron microscopy (TEM) and atomic force microscopy (AFM) revealed that the mean length of SWCNTs and lateral size of GO were 902 ± 126 nm and 412 ± 87 nm (*SI Appendix*, Fig. S1 *A–D*), respectively. X-ray photoelectron spectrum indicated a high oxidation level of the SWCNTs (C–O, 30.36%; COOH, 6.05%) and the GO (C–O, 42.36%; COOH, 8.71%) (*SI Appendix*, Fig. S1 *E* and *F*).

Once CNMs are administered via an oral route, they will encounter trillions of gut microbes in the gut lumen. Because the structure unit of CNMs is carbon element, we hypothesize that they might serve as an available carbon source and become involved in a number of product syntheses through microbial fermentation. Normally, the major products from the microbial fermentative activity in the gut are short-chain fatty acids (SCFAs) (23). To explore the end products of microbial CNM fermentation, we collected the supernatants of CNMs-treated gut bacteria and screened a series of SCFAs including acetate, propionate, butyrate, valeric acid (VA), and caproic acid (CA) in vitro by high-performance liquid chromatography (HPLC). Fig. 1*A* shows that SWCNT- and GO-treated gut bacteria produced substantial amounts of butyrate (~1.1 mM), a low level of acetate (~0.2 mM) (using derivation method as shown in *SI Appendix*, Fig. S2), and undetectable levels of propionate, VA, and CA in vitro. At animal

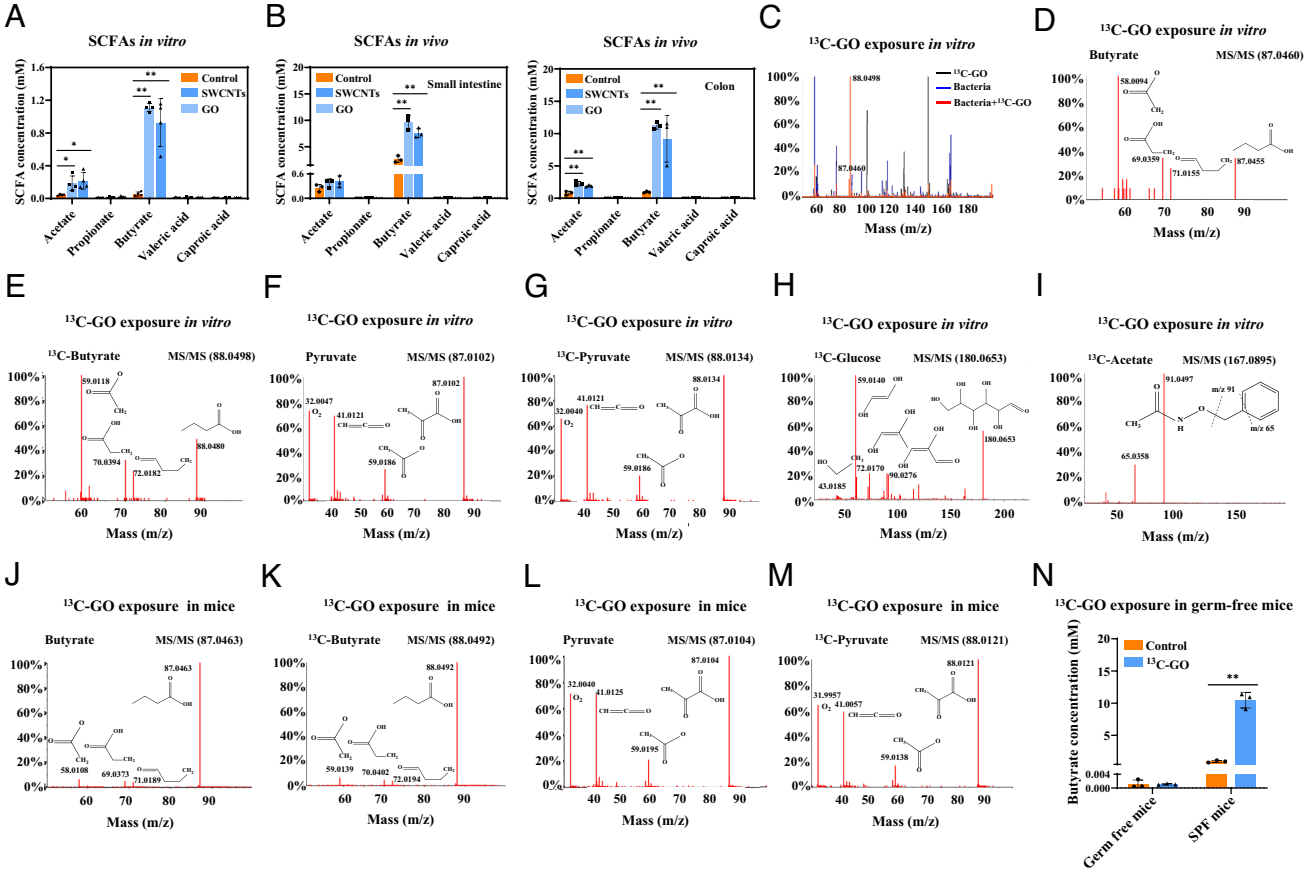

Fig. 1. The gut microbiota ferments inorganic carbon nanomaterials as an available carbon source into butyrate through the pyruvate pathway. (*A* and *B*) SCFAs contents in CNM-treated gut bacteria in vitro (*A*) and CNM-treated mice (*B*) analyzed by HPLC. For in vitro experiment, gut bacteria (1×10^9 cells) were incubated with CNMs (0.05 mg/mL) for 3 d in anerobic condition, and the supernatants of gut bacteria samples were collected to assess SCFAs levels (n = 4, four replicates). For in vivo experiment, the intestinal contents were collected to assess local SCFAs levels in the small intestine (ileum) and colon of mice treated with SWCNTs (2.5 mg/kg/day) and GO (2.5 mg/kg/day) by oral gavage for 28 d (n = 4, biologically independent mice). (*C*) MS spectra of ^{13}C–GO, bacteria, and ^{13}C–GO-treated bacteria as determined by ultrahigh performance liquid chromatography-triple time-of flight mass spectrometry (UHPLC-Triple TOF-MS). (*D* and *E*) Characteristic fragment ions of butyrate (*D*) and ^{13}C-butyrate (*E*) in the supernatant of ^{13}C–GO-treated bacteria. (*F* and *G*) Characteristic fragment ions of pyruvate (*F*) for ^{13}C-pyruvate (*G*) in the lysate of gut bacteria treated with ^{13}C–GO. (*H*) MS/MS spectra of ^{13}C-glucose in the lysate of gut bacteria treated with ^{13}C–GO. (*I*) MS/MS spectra of ^{13}C-acetate determined by derivation method using UHPLC-Triple TOF-MS. (*J–M*) MS/MS spectra of butyrate (*J*), ^{13}C-butyrate (*K*), pyruvate (*L*), and ^{13}C-pyruvate (*M*) in the colon of mice treated with ^{13}C–GO (2.5 mg/kg/day) by oral gavage for 28 d. (*N*) ^{13}C–GO (2.5 mg/kg/day) induced significant increase of butyrate in the SPF mice but not GF mice (n = 3, biologically independent mice). Data are expressed as mean ± SD. Statistical significance was tested with two tailed *t* test and one-way ANOVA analysis. $^*P < 0.05$, $^{**}P < 0.01$.

level (no significant alteration in general health status in CNM-treated mice as shown in *SI Appendix*, Fig. S3), the amounts of butyrate in the small intestine of SWCNT- and GO-treated mice were 3.8- and 2.9-fold higher than control, whereas the levels of butyrate in the colon of SWCNT- and GO-treated mice were 11.8- and 9.7-fold higher than control (Fig. 1*B*). While we also observed elevated acetate in the CNM-treated mice (Fig. 1 *B*, *Right*), its concentration was much lower than that of butyrate. Other SCFAs (propionate, VA, and CA) were not significantly changed in CNM-treated mice. These data suggested that butyrate was the major product of microbial CNMs fermentation.

To track whether butyrate was derived from the CNMs fermentation, we used the state-of-the-art stable isotope tracing technique to reveal the metabolite flux of ^{13}C-labeled GO [^{13}C–GO was synthesized by the arc discharge method (36)] in gut bacteria. *SI Appendix*, Fig. S4*A* shows that gut bacteria incubated with ^{13}C–GO produced butyrate, in agreement with the results in Fig. 1*A*. The mass spectrometry (MS) spectra showed a presence of parent ions of m/z 87.046 and 88.049 in the supernatant of gut bacteria treated with ^{13}C–GO (Fig. 1*C*, Red line). Because they show the same fragment ions pattern as the butyrate standard (*SI Appendix*, Fig. S4 *B* and *C*), these two parent ions were identified to be butyrate and ^{13}C-butyrate, respectively (Fig. 1 *D* and *E*), indicating that gut bacteria exploited either nutrients or CNMs in culture medium as a carbon source for butyrate biosynthesis. Importantly, the intensity of ^{13}C-butyrate was ~sixfold higher than butyrate in Fig. 1*C*, suggesting that CNMs were fermented into butyrate as an available carbon source in gut bacteria. To further explain the phenomenon of ^{13}C-butyrate was higher than ^{12}C-butyrate, we performed density functional theory calculations to calculate the different dissociation energies of ^{12}C and ^{13}C from GO (GO cluster model was used) (*SI Appendix*, Fig. S4*D*). The more negative ΔG_2 (−667.52 kJ/mol) was than ΔG_1 (−665.35 kJ/mol) suggested that ^{13}C was thermodynamically easier to be dissociated from GO than ^{12}C, which supported the previous findings that ^{12}C–^{13}C bond was weaker than the ^{12}C–^{12}C bond (37, 38). These data imply that when the ^{13}C–GO was subjected to the reaction of butyrate biosynthesis, the ^{13}C was probably easier to be dissociated from GO than ^{12}C. Therefore, the bacteria can exploit more ^{13}C for butyrate synthesis than ^{12}C.

We next probed into the fermentation process of CNMs in gut microbiota by analyzing the precursors of butyrate. Because the pyruvate pathway is the most important fermentation pathway to produce SCFAs (23), we expected that CNMs were fermented into butyrate through the pyruvate pathway. As expected, we confirmed the presence of pyruvate and ^{13}C-pyruvate in the lysate of gut bacteria treated with ^{13}C–GO for 3 d (Fig. 1 *F* and *G* and *SI Appendix*, Fig. S4*E*), which are the upstream precursors of butyrate and ^{13}C-butyrate, respectively. We also found the ^{13}C-glucose (the precursor of pyruvate) and phosphoenolpyruvate (PEP, the downstream product of glucose) in the ^{13}C–GO-treated bacteria (Fig. 1*H* and *SI Appendix*, Fig. S4 *F* and *G*). It is notable that most butyrate producers can also generate acetate through pyruvate metabolism as a major fermentation product along with butyrate (39). Interestingly, we identified the acetate and ^{13}C-labeled acetate in the supernatant of gut bacteria treated with ^{13}C–GO using the derivation method (Fig. 1*I* and *SI Appendix*, Fig. S4 *H–J*), implying that acetate might act as a precursor for butyrate production. In addition, the presence of butyrate, ^{13}C-butyrate, pyruvate, and ^{13}C-pyruvate in the gut lumen of mice treated with ^{13}C–GO (2.5 mg/kg/day) for 28 d (Fig. 1 *J–M*) indicated that CNMs were fermented into butyrate through the central pyruvate pathway. Of note, we did not observe two or more ^{13}C incorporation in these products, which was highly dependent on the label ratio of ^{13}C in GO (The label ratio was 9.88%, the probability of having one ^{13}C incorporation in butyrate is 28.9%, which was almost two and three orders of magnitude of two, three, and four ^{13}C incorporation in butyrate.) (*Materials and Methods*). Meanwhile, we also used germ-free (GF) mice to corroborate the effects of the gut microbiota on butyrate production. Indeed, the absence of the gut microbiota completely abrogated ^{13}C–GO-increased butyrate production in GF mice compared to the observed effect in SPF mice (Fig. 1*N*), confirming the pivotal role of the gut microbiota on butyrate biosynthesis and ruling out contributions of other factors (such as gut epithelium) to the excessive butyrate generated by the CNMs in the gut.

The Bacterial Enzymes Involved in the CNMs Fermentation into Butyrate through Pyruvate Pathway. CNMs fermentation is a multistep process carried out by gut microbiota. Normally, the microbial conversion of CNMs from pyruvate to butyrate involves a number of principal reactions mediated by the key enzymatic repertoire of the gut microbiota (40). We found that ^{13}C–GO dramatically increased the activity of hexokinase (Fig. 2*A*), pyruvate kinase (PK) (Fig. 2*B*), and pyruvate dehydrogenase (PDH) (Fig. 2*C*) and the amounts of acetyl-CoA, butyryl CoA, butyrate kinase, and butyryl-CoA: acetyl-CoA transferase (BUT) in the gut bacteria (1×10^8 bacteria) (Fig. 2 *D–G*). In the biosynthetic pathway of butyrate, hexokinase plays an important role in catalyzing glucose phosphorylation with the consumption of adenosine triphosphate (ATP) to further produce PEP (41, 42) and PK catalyzes PEP to produce the pyruvate. PDH catalyzes the conversion of pyruvate to acetyl-CoA with the involvement of CoA and condensation of two molecules of acetyl-CoA forms butyryl-CoA that is further converted to butyrate via the classical pathway through butyrate kinase (40). In addition, butyryl-CoA can yield to butyrate by the butyryl-CoA:acetate CoA-transferase route or with the addition of acetate (acetate is produced from the upstream acetyl-CoA) (43). Of note, the unchanged I_D/I_G of ^{13}C–GO incubated with pure enzymes (PDH or butyrate kinase) (*SI Appendix*, Fig. S5) indicated that these enzymes were involved in the conversion between butyrate and its upstream product, pyruvate, but not directly acted on CNMs per se. Apart from the ^{13}C–GO, we also found similar behavior of SWCNTs and GO on the bacterial enzymes, increasing the activity of hexokinase, PK, and PDH and the amounts of acetyl-CoA, butyryl CoA, butyrate kinase, and BUT in the gut bacteria (Fig. 2 *H–N*). These combined results (Figs. 1 and 2 *A–N*) suggested that CNMs altered the metabolite profile of gut microbiota that switched to other available sources exploiting inorganic CNMs in fermentation, to synthesize organic butyrate through the central pyruvate pathway (Fig. 2*O*).

Gut Microbiota Degrades Carbon Nanomaterials. In general, the premise of CNMs fermentation is the degradation of particles. Although several clues have demonstrated the degradation of CNMs by environmental aerobic microbes (30–34), it is still unknown whether gut microbiota are capable of degrading CNMs because 99% gut microbiota is obligate anaerobes. To solve this issue, we extracted fresh gut bacteria from the colon and incubated them with the SWCNTs and GO at an appropriate dose of 0.05 mg/mL for 3 d (Fig. 3*A*). We first studied changes of the nanoparticle size using sodium dodecyl sulfate-polyacrylamide gel electrophoresis (SDS-PAGE). There was no dark band inside gel for the bacteria control (Fig. 3 *B*, *Left*). SWCNTs and GO were only observed at the interface between the loading well, appearing as two distinctive dark bands (Fig. 3 *B*, *Middle*). However, after incubation with gut bacteria, the fragments of SWCNTs and GO were detectable in the lower gel (Fig. 3 *B*, *Right*). SDS-PAGE

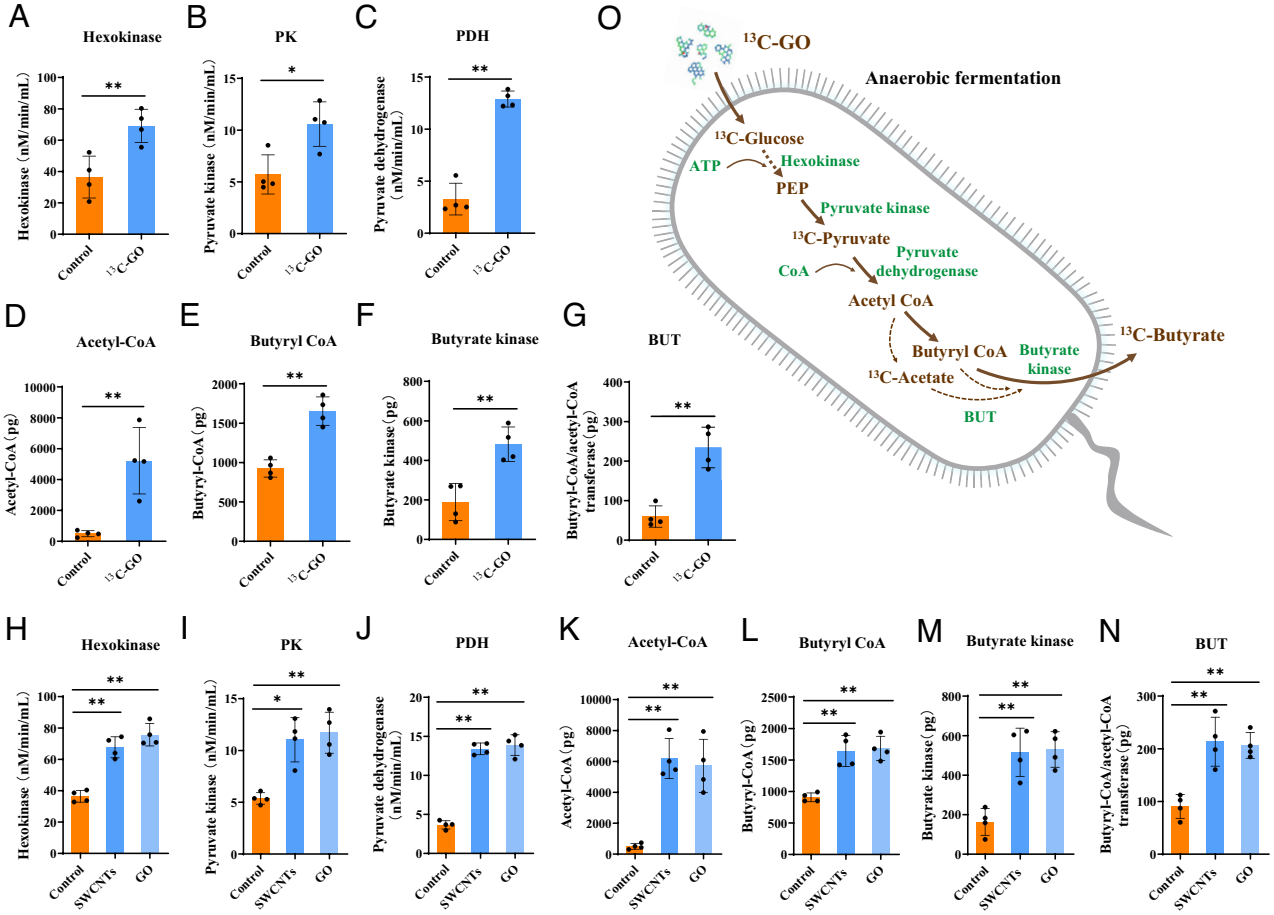

Fig. 2. The bacterial enzymes involved in the CNMs fermentation. (*A–C*) ^{13}C–GO induced the increased hexokinase activity (*A*), PK activity (*B*), and PDH activity (*C*) in gut bacteria (n = 4, four replicates, 1 × 10^8 bacteria for each group). (*D–G*) ^{13}C–GO induced the increased amount of acetyl-CoA (*D*), butyryl CoA (*E*), butyrate kinase (*F*), and butyryl-CoA: acetyl-CoA transferase (*G*) in gut bacteria (n = 4, four replicates, 1 × 10^8 bacteria for each group). (*H–J*) SWCNTs and GO induced the increased hexokinase activity (*H*), PK activity (*I*), and PDH activity (*J*) in gut bacteria (n = 4, four replicates, 1 × 10^8 bacteria for each group). (*K–N*) SWCNTs and GO induced the increased amount of acetyl-CoA (*K*), butyryl CoA (*L*), butyrate kinase (*M*), and butyryl-CoA: acetyl-CoA transferase (*N*) in gut bacteria (n = 4, four replicates, 1 × 10^8 bacteria for each group). (*O*) Schematic illustrating that ^{13}C–GO was transformed into butyrate through the pyruvate pathway and relevant enzymes by bacterial fermentation. Data are expressed as mean ± SD. Statistical significance was tested with two tailed *t* test and one-way ANOVA analysis. **P* < 0.05, ***P* < 0.01.

is analogous to a molecular sieve; it can screen different-sized biomolecules and particles reaching different depths of the gel based on their molecular weight. The presence of nanoparticles in the lower gel indicated their degradation.

As degradation of CNMs was expected to be accompanied by structural damage, we used Raman spectroscopy to verify the defect sites in the CNMs (GO had similar D band and G band with ^{13}C–GO in *SI Appendix*, Fig. S6). After incubation with gut bacteria, Raman spectra exhibited an increased ratio of the D-band (1,340 cm^{-1}) to the G-band (1,580 cm^{-1}) intensity for SWCNTs (I_D/I_G = 0.43) and GO (I_D/I_G = 1.00), compared to the SWCNTs (I_D/I_G = 0.28) and GO (I_D/I_G = 0.63) in a culture medium (Fig. 3 *C* and *D*). Since the D-band represents a disorder-induced mode due to asymmetry-increasing effects (such as defects in the sp^2 hybridized carbon systems) (26, 29), the increased I_D/I_G suggested an increase in defect sites and structural damage to the SWCNTs and GO. The greater value of I_D/I_G for GO incubated with gut bacteria, compared with SWCNTs under the same condition, indicated a more effective degradation of the structurally more accessible nanosheets by the microorganisms. We further conducted matrix-assisted laser desorption/ionization time-of-flight (MALDI-TOF) mass spectrometry to analyze the ion currents of the CNMs in positive ionization mode. SWCNTs displayed high-intensity mass-to-charge (m/z) peaks at approximately 47,000 to 59,000, whereas the SWCNTs treated with gut bacteria showed sharply different characteristics with m/z ratios ranging from 2,000 to 25,000 and multiple peaks of high intensities (Fig. 3*E*). A similar observation was made for the GO and GO/bacteria group (Fig. 3*F*). The presence of lower m/z peaks and a lack of signal at 47,000 to 59,000 were indicative of fragmentation and shortening of the nanotubes and nanosheets. Furthermore, microscopy analysis revealed that the characteristic fibrillary structure of the nanotubes was destroyed and the bulk of nanotubes no longer existed after the bacteria treatment (Fig. 3 *G*, *Upper*). Indeed, we observed abundant nanotube debris. Similarly, AFM imaging showed prominent pitting and fragments in the bacteria-treated GO (Fig. 3 *G*, *Lower*), suggesting that gut bacteria effectively degraded CNMs structurally.

To study how gut bacteria degrade CNMs, we conducted the degradation experiment using heat-killed bacteria and spent bacterial medium and compared the I_D/I_G change of the CNMs by Raman spectroscopy. There were no significant changes to the defect sites of SWCNTs and GO treated with heat-killed bacteria or spent bacterial medium compared to the SWCNTs and GO in the culture medium (Fig. 3 *H* and *I*), indicating that inactive bacteria, microbial fermentation products, or acidification of the media did not elicit CNMs degradation. In contrast, active gut bacteria induced a significant increase of CNMs defect sites. These

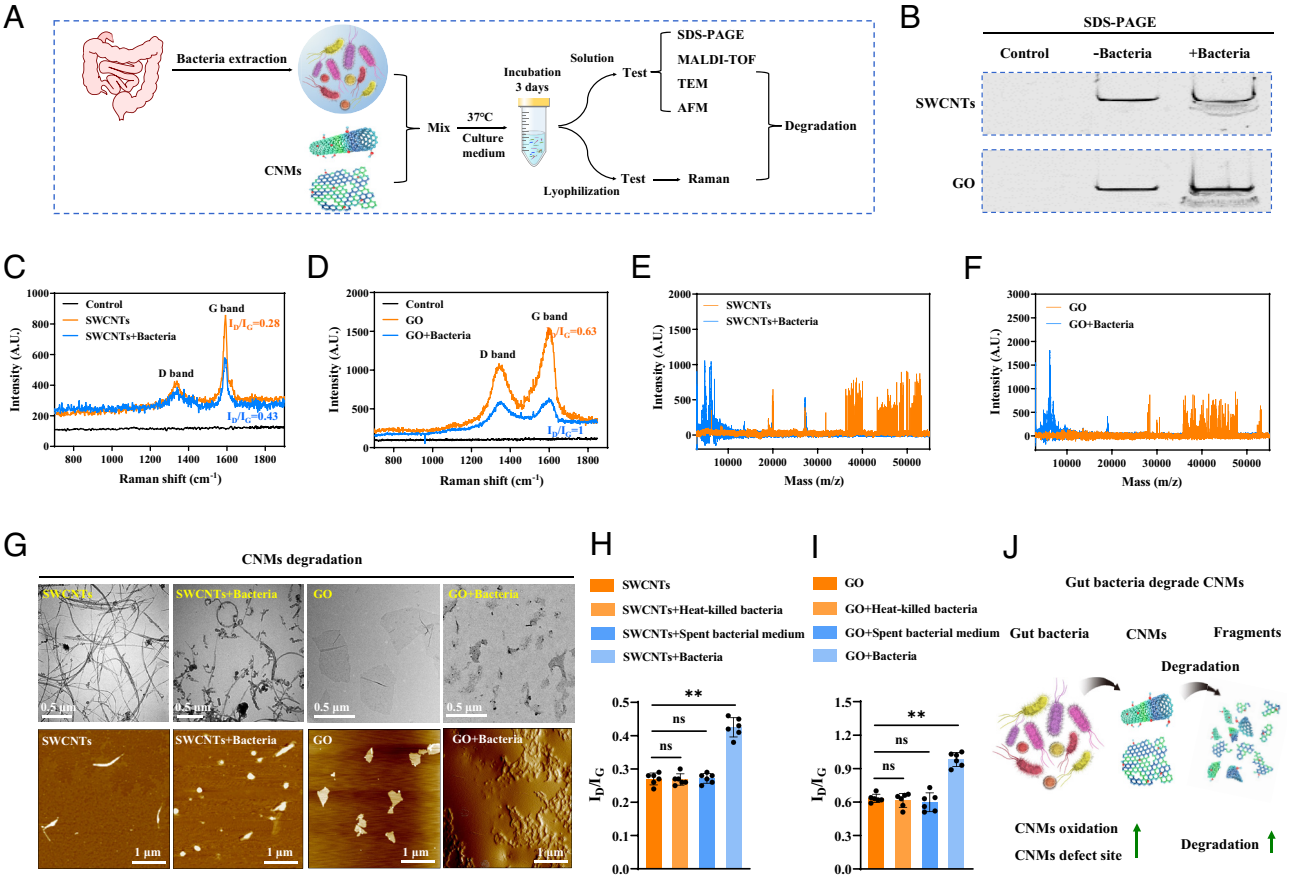

Fig. 3. The gut microbiota degrades carbon nanomaterials. (*A*) Experimental design for the degradation of CNMs by gut bacteria. Freshly isolated gut bacteria (1×10^9 cells for each group) were treated with SWCNTs (0.05 mg/mL) and GO (0.05 mg/mL) for 3 d in anaerobic condition [we used a pool of colon fecal extracts from multiple mice (n=10) for all in vitro experiments]. The different samples were then determined by various tests. (*B*) SDS-PAGE analysis of the mobility of SWCNTs and GO treated with or without gut bacteria. The gut bacteria alone were set as control. (*C* and *D*) Raman spectra of SWCNTs (*C*) and GO (*D*) incubated with or without gut bacteria, showing decreased G-bands, followed by the appearance and decay of D-bands. I_D: intensity of the D-band; I_G: intensity of the G-band. The gut bacteria alone were set as control. The spectra are representative of six independent experiments. (*E* and *F*) MALDI-TOF mass spectrometry analysis for the ion currents of SWCNTs (*E*) and GO (*F*) incubated with or without gut bacteria. (*G*) Representative TEM and AFM images confirming the degradation of SWCNTs and GO induced by gut bacteria. (*H* and *I*) The I_D/I_G ratio of SWCNTs (*H*) and GO (*I*) in tested samples. SWCNTs and GO were incubated with heat-killed bacteria (gut bacteria were inactivated at 75 °C for 60 min in water bath), spent bacterial medium (gut bacteria were cultured in medium for 3 d and the supernatants were collected through centrifugation termed as spent bacterial medium), and active gut bacteria for 3 d; the I_D/I_G of CNMs was then determined by Raman spectroscopy (n = 6, six replicates). (*J*) Schematic illustration of CNMs degradation by gut microbiota. Data are expressed as mean ± SD. Statistical significance was tested with two tailed *t* test and one-way ANOVA analysis. $^{**}P < 0.01$, ns means no statistical significance.

evidence clearly pointed to gut bacterial metabolism (only available in active bacteria) as a cause for CNMs degradation.

Because the biological components in gut lumen are critical to the fate of invading nanomaterials, we explored the impact of pancreatin on the degradation of CNMs using simulated intestinal fluid (SIF). As illustrated in *SI Appendix,* Fig. S7, there were no obvious changes to the size and morphology of the CNMs incubated with SIF for 3 d, indicating that pancreatin did not participate in the degradation of the CNMs. Since material, oxidation degree, and particle size have been suggested as key parameters for the degradation of nanoparticles in biological systems (29, 44, 45), we therefore investigated the structure–effect relationship using a series of nanoparticles (NPs), including TiO_2 NPs, carbon black (CB) NPs, pristine SWCNTs (with lower oxidation compared to SWCNTs), short SWCNTs (obtained by the sonication of SWCNTs), graphene (with lower oxidation compared to GO), and small GO (obtained by the sonication of GO) (*SI Appendix,* Table S1; the addition of surfactant did not influence the bacteria viability, as shown in *SI Appendix,* Fig. S8). We found that both TiO_2 and CB were not degraded by gut bacteria (*SI Appendix,* Fig. S9*A*; there was no butyrate production induced by TiO_2 and CB in gut bacteria in *SI Appendix,* Fig. S9*B*), suggesting that material was a key element to dictate the degradation behavior of nanoparticles by gut bacteria. Notably, when the particle size decreased, the oxidation degree (O/C) and defect site (I_D/I_G ratio) of the CNMs increased and gut bacteria–governed CNMs degradation and butyrate production enhanced accordingly (Fig. 3*J* and *SI Appendix,* Fig. S9 *A–C*). Given these facts, the structure–effect relationship is dependent on the physicochemical properties of the nanomaterial and at least in part is specific to graphene-based nanoparticles. The basic structure of graphene-based nanoparticles is aromatic rings fused by sp^2-hybridized carbon, which is considered stable. However, the abundant oxidation and defect sites in SWCNTs and GO may provide targets via their dangling bonds and surface carboxyl, hydroxyl, and epoxy groups for the attack by gut bacteria.

Identification of Dominant Gut Bacteria Fermenting CNMs for Butyrate Synthesis. We further explored which specific bacteria were dominant in preference for the CNMs as their carbon source. For in vitro experiments, we used a pool of bacterial extracts from multiple mice (n = 10). We first monitored the microbial composition of bacterial extracts before their CNMs exposure by 16S ribosomal RNA (rRNA) gene sequencing. The sequencing

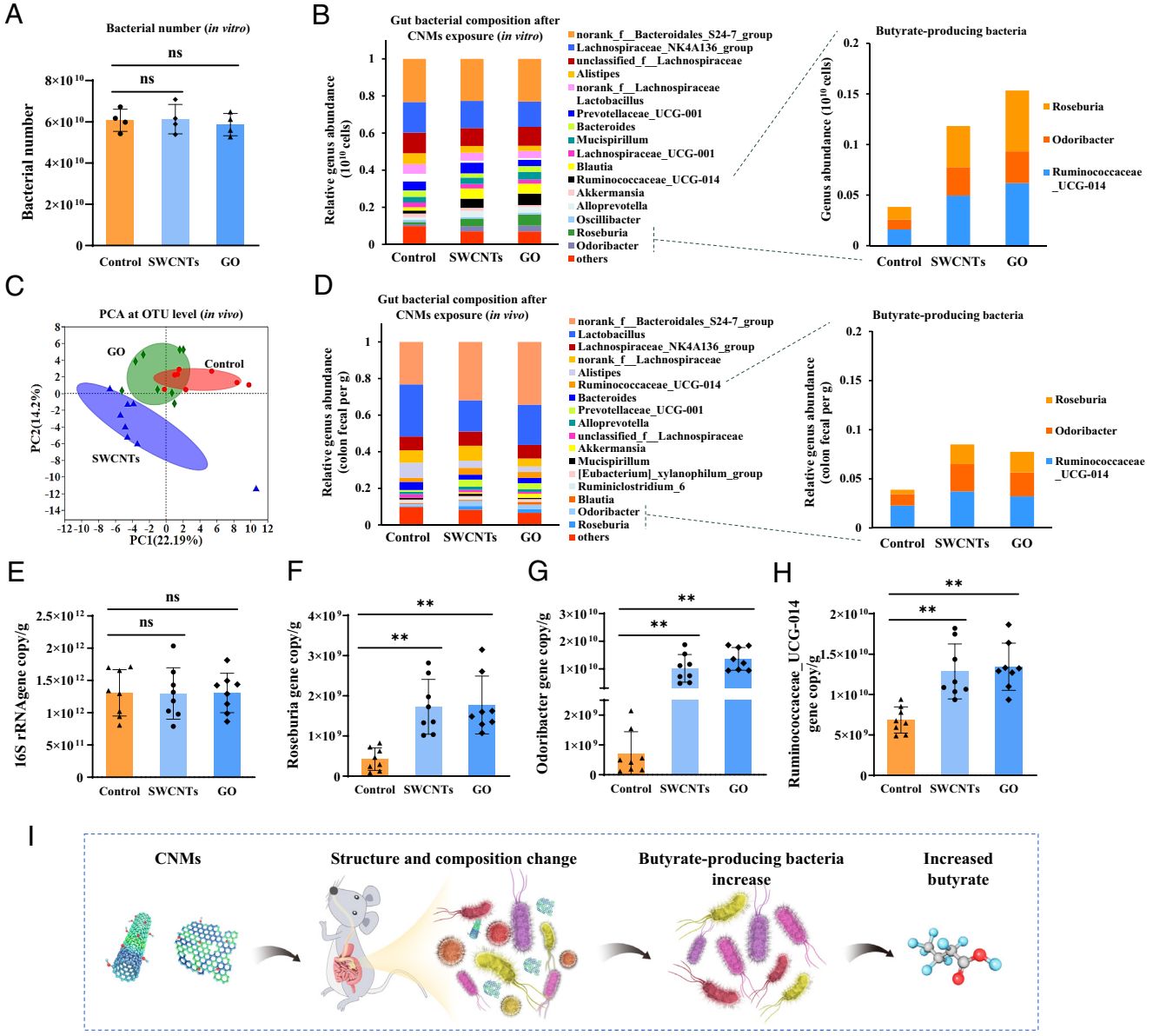

Fig. 4. CNMs alter the structure of the gut microbiota and increase the abundance of butyrate-producing bacteria. (*A*) Bacterial number in control, SWCNT- and GO-treated bacteria, as determined by bacterial counter (n = 4, four replicates). (*B*) Relative abundance of gut bacteria in control, SWCNTs and GO group at genus level in vitro. After CNMs (0.05 mg/mL) exposure for 3 d in anerobic condition, same number bacteria (1×10^{10} cells) for each group were subjected to gene sequencing (n = 4, four replicates). The top 17 most abundant genera are depicted, with all others pooled into "other." (*C*) PCA plots of gut microbiota in control and CNM-treated mice (n = 8, biologically independent mice). (*D*) Relative abundance of gut bacteria in control and CNM-treated mice. The mice were treated with CNMs (2.5 mg/kg/day) by oral gavage for 28 d; same amount of colon fecal (1 g) was collected for 16s rRNA gene sequencing at genus level (n = 8, biologically independent mice). (*E–H*) Absolute quantification of 16S rRNA gene copy number of total gut bacteria (*E*), Roseburia (*F*), Odoribacter (*G*), and Ruminococcaceae_UCG-014 (*H*) in same amount of colon fecal (1 g) in mice (n = 8, biologically independent mice). (*I*) Schematic illustrating that CNMs alter the structure of gut bacteria and increase the abundance of butyrate-producing bacteria. Data are expressed as mean ± SD. Statistical significance was tested with two tailed *t* test and one-way ANOVA analysis. $^{**}P < 0.01$, ns means no statistical significance.

data exhibited identical bacterial features including diversity and composition for three groups (*SI Appendix*, Fig. S10 *A* and *B*). After CNMs (0.05 mg/mL) exposure, SWCNTs and GO did not influence bacterial viability and total number compared to control (Fig. 4*A* and *SI Appendix*, Fig. S10*C*), indicating that CNMs were not antimicrobial to the total number of microbes. We next determined the genera abundance in different treatments using same microbial loads (1×10^{10} cells) and rarefying sequencing output to an equal number of reads per sample, which allowed a comparison between control and CNM-treated group (46). Interestingly, SWCNTs and GO reduced the diversity of the gut microbiota (*SI Appendix*, Fig. S10*D*) showing decreased Alistipes and Lactobacillus but increased butyrate-producing bacteria (major function is to produce butyrate) including Roseburia, Odoribacter, and Ruminococcaceae (Fig. 4*B*). It was clear that CNMs did not impact the total microbial number compared to control, whereas they selectively promoted the growth of butyrate-producing bacteria, thus altering the composition of the gut microbiota.

At animal level, we carefully evaluated the gut microbiota composition using same amount of fecal before CNMs exposure. The gut microbiota displayed a similar diversity and composition between different groups (*SI Appendix*, Fig. S11 *A* and *B*). After CNMs exposure, the diversity of the gut microbiota was reduced (*SI Appendix*, Fig. S11*C*). Particularly, SWCNTs and GO significantly shifted the bacterial community as manifested in principal

coordinate analysis (PCA) (Fig. 4*C*), suggesting that CNMs changed the constitution of the gut microbiota. To discern which gut bacteria were changed, we further investigated the bacterial composition at genus level. Approximately 9 and 5 genera were reduced in SWCNT- and GO-treated mice, respectively (Fig. 4 *D*, *Left*). Consistent with the in vitro data, Alistipes and Lactobacillus were reduced in response to CNMs exposure, while total butyrate-producing bacteria (including Roseburia, Odoribacter, and Ruminococcaceae) increased from 3.8% in the control to 8.5% and 7.7% in SWCNT- and GO-treated mice, a ~2.2-fold elevation in CNM-treated mice over control (Fig. 4 *D*, *Right*). Of note, CNMs promoted the increase of butyrate-producing bacteria in a time-dependent manner (*SI Appendix,* Fig. S11*D*).

Furthermore, we performed absolute quantification of 16S rRNA gene copy to compare the microbial number change between control and CNM-treated mice using same amount of colon fecal. The 16S gene copy number of total gut bacteria was almost identical between control and CNM-treated mice (Fig. 4*E*, primers are listed in *SI Appendix,* Table S2), indicating that CNMs did not influence the total number of microbes in the intestine. Hence, we could compare changes to the genera abundance between different groups using same amount of colon fecal. We also performed absolute quantification of butyrate-producing bacteria by constructing corresponding plasmids and examining their gene copy numbers, expressed as gene copy number per gram of colon fecal. The results revealed that SWCNTs and GO promoted the growth of butyrate-producing bacteria including Roseburia, Odoribacter, and Ruminococcaceae (Fig. 4 *F*–*H*). This exhibited a similar trend with the butyrate-producing bacteria using relative microbiome analyses (Fig. 4*D*). All data indicate that CNMs altered the structure and composition of the gut microbiota. Nevertheless, there was a compensation mechanism to maintain the dynamic balance of total microbial number, where the reduction of certain bacteria was compensated by increased butyrate-producing bacteria (Fig. 4*I*).

The gene sequencing results also exhibited decreased Firmicutes but increased Bacteroidetes at phylum level (*SI Appendix,* Fig. S11*E*). Recent studies have demonstrated that Firmicutes possesses higher efficiency in food fermentation and calories absorption than Bacteroidetes (47, 48). Accordingly, function analysis revealed that CNMs attenuated the carbohydrate transport and metabolism capacity of total gut bacteria, dropping from 15.9% in control to 9.6% and 11.3% in SWCNT- and GO-treated mice (*SI Appendix,* Fig. S12*A*). However, in contrast to total gut bacteria, the butyrate-producing bacteria exhibited an opposite effect, with a sixfold elevation in carbohydrate transfer and metabolism in CNM-treated mice (*SI Appendix,* Fig. S12*B*). Because these gut bacteria are highly enriched for genes involved in energy production and metabolism, that will help facilitate the host's ability to extract calories from their diet, thus maintaining the gut homeostasis (49, 50). In our case, CNMs were an unconventional diet/source for butyrate-producing bacteria. As a community of bacteria, these multispecies bacteria might cooperate with each other for the breakdown of CNMs and exploit the CNMs for their growth and butyrate production. Together, these data provided compelling evidence that although butyrate-producing bacteria accounted for a small proportion (~4 to 15%) of total gut bacteria, they were the dominant bacteria fermenting CNMs as a bioavailable carbon source to produce butyrate.

CNMs Influence Intestinal Stem Cells through Their Transformed Butyrate by Microbial Fermentation. The fermentation of CNMs contributed to the overproduction of butyrate by butyrate-producing bacteria. An open question remains: what are the biological consequences of these transformed CNMs in the gut? Because excessive butyrate is detrimental to the renewal of gut epithelium that is driven by LGR5$^+$ intestinal stem cells (ISCs) (51, 52), we speculated that CNMs might cooperate with gut bacteria to influence the ISCs function through producing excessive butyrate. To test this, we assessed the proliferation of ISCs labeled with LGR5 antibody by flow cytometry. As expected, CNMs (2.5 mg/kg/day) dramatically inhibited LGR5$^+$ ISCs proliferation in the colon and small intestine of mice compared to control (Fig. 5 *A* and *B*). To further verify whether the inhibitory effect of CNMs on ISCs was mediated by the overproduction of butyrate, the mice were directly exposed to butyrate (5 mM, 10 mM) by oral gavage for 3 d. Butyrate inhibited LGR5$^+$ ISCs proliferation in a dose-dependent manner in the colon and small intestine (Fig. 5 *C* and *D*). In fact, butyrate can only be produced by the fermentative activity of commensal gut microbiota in host (23). In the absence of the gut microbiota, CNM-induced inhibition of LGR5$^+$ ISCs proliferation was completely ablated in either GF mice (Fig. 5*E*) or intestinal organoids [an in vitro GF system, the crypt where ISCs reside was employed for organoid culture (53)] (*SI Appendix,* Fig. S13*A*). In contrast, butyrate (5 mM) alone showed a suppressed effect on LGR5$^+$ ISCs proliferation in GF mice (*SI Appendix,* Fig. S13*B*) and intestinal organoids (*SI Appendix,* Fig. S13*C*), whereas the addition of SWCNTs and GO did not enhance this inhibitory effect of butyrate. Furthermore, the immunofluorescence analysis also exhibited that butyrate suppressed the proliferation (Ki67) of intestinal cells and the differentiation of ISCs into goblet cells (Mucin 2) in mice (Fig. 5*F*) and organoids (Fig. 5*G*). The butyrate-treated organoids exhibited distinctly different morphology to control, showing the loss of intestinal villi, whereas CNMs alone did not influence the formation of intestinal villi in organoids (Fig. 5*G* and *SI Appendix,* Fig. S13*D*). These data indicated that CNMs inhibiting ISCs function was due to their transformed butyrate indirectly acting on the ISCs (Fig. 5*H*).

So far, we have shown that CNMs fermentation induced increased butyrate. Normally, butyrate has pleiotropic effects, including acting as energy source of colonocyte to regulate the metabolism through G protein-coupled receptor (54), reinforcing the gut barrier (55, 56) or immunomodulation in the gut (57). We showed the inhibitory effect of butyrate on stem cell proliferation, which was consistent with a previous study (51). They revealed that the intact architecture of intestinal villi protected the stem cells from the influence of butyrate. However, the disrupted intestinal villus induced by CNMs (*SI Appendix,* Fig. S14 *A*–*E*) resulted in stem cells inside the base losing the protection. As a result, the excessive butyrate can directly act on and inhibit the proliferation of intestinal stem cells, again indicating that the influence of CNMs on butyrate levels is sufficient to mediate a biological effect. Although inhibition of ISCs function only represented one mechanism within the complex network of nano–microbiota interactions, these results shed light on how CNMs regulated the function of neighboring ISCs through their interplay with the gut microbiota. Of course, in spite of their negative effect, future studies are warranted to investigate whether these changes in butyrate also lead to other biological effects (e.g., regulating metabolism and gut barrier) and their influence in butyrate-dependent disease models of colitis, allergy, and colorectal cancer.

Conclusions

Recent literature has increasingly implicated the gut microbiota as central to human health, regulating the body homeostasis directly or holistically via the gut-centric axes and contributing to the physiopathologies of diverse diseases (19, 20). Due to its vast

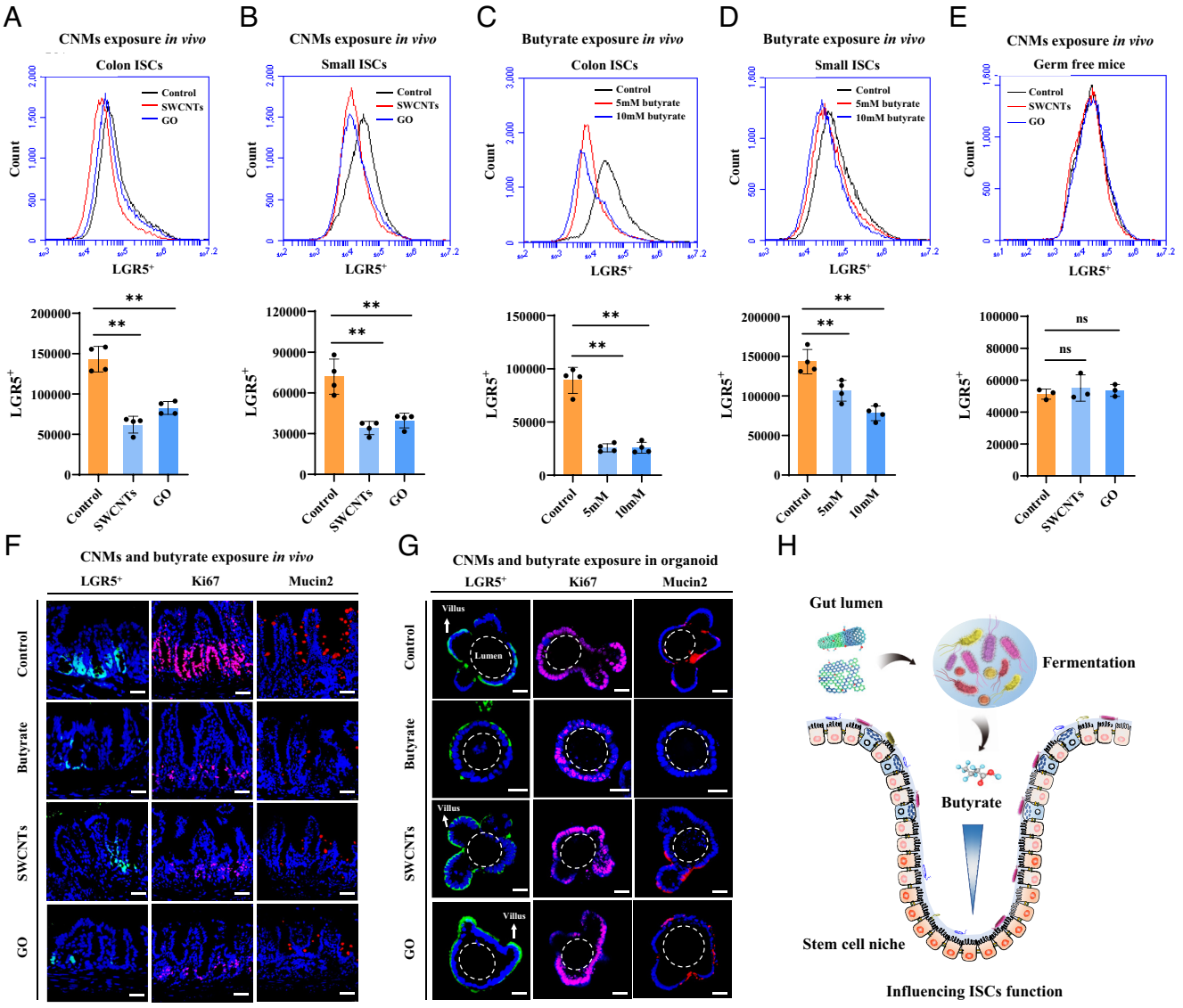

Fig. 5. CNMs impact the function of intestinal stem cells through butyrate transformed by microbial fermentation. (*A* and *B*) SWCNTs and GO (2.5 mg/kg/day) inhibited the proliferation of LGR5$^+$ ISCs in the colon (*A*) and small intestine (*B*) of mice by oral gavage for 28 d (n = 4, biologically independent mice). (*C* and *D*) Butyrate inhibited the proliferation of LGR5$^+$ ISCs in the colon (*C*) and small intestine (*D*) of mice treated with butyrate (5 mM and 10 mM) by oral gavage for 3 d (n = 4, biologically independent mice). (*E*) SWCNTs and GO (2.5 mg/kg/day) had no effect on the proliferation of LGR5$^+$ ISCs in the colon of GF mice for 28 d (n = 3, biologically independent mice). (*F*) Representative immunostaining showing the effects of butyrate (5 mM), SWCNTs and GO on the ISCs (LGR5$^+$, green), proliferated cells (Ki67, red) and goblet cells (Mucin 2, red) in colon of mice (n = 4, four replicates). (Scale bar: 50 μm.) (*G*) Representative immunostaining showing the effects of butyrate, SWCNTs and GO on the differentiation of intestinal organoid. (Scale bar: 50 μm.) The images are representative of three independent experiments. (*H*) Schematic illustrating that CNMs influence the function of ISCs through their transformed butyrate. Data are expressed as mean ± SD. Statistical significance was tested with two tailed *t* test and one-way ANOVA analysis. $^{**}P < 0.01$, ns means no statistical significance.

complexity and entanglement with the entire human anatomy, the gut microbiota has remained to date a largely uncharted territory to the exploration of nanomedicine, nanosafety, and nanotoxicology. Accordingly, the current study made a breakthrough by providing an analytical framework for obtaining unique insights into the fundamental biological processes and consequences of CNMs dominated by gut microbiota in their hosts. We evaluated the life cycle of CNMs in the gut environment where trillions of gut microbiota reside. Our results collectively demonstrated the degradation, transformation, and fermentation of CNMs, the aspects closely associated with the biological consequences of CNMs in the gut (Fig. 6) (and beyond).

At the very beginning of CNMs turning into glucose, CNMs were first degraded into small fragments along with the decreases of size and m/z and increased number of defect sites (Fig. 3). Although there are no available techniques capable of identifying the specific molecular structure of CNMs fragments, in this process, the carbon atom was thermodynamically easier to dissociate from CNMs that can be ultimately used for the synthesis of glucose. Importantly, we revealed that the gut microbiota fermented inorganic CNMs as a bioavailable carbon source into organic butyrate through the pyruvate pathway during CNMs fermentation, which serves as a key process of a delicate ecological balance that drives nanoparticles removal in gut microenvironment, thereby entailing a new biological fate and identity of CNMs in mammals and breaking the current knowledge system that microbes only use organic compounds for the synthesis of organic butyrate. Although the precise mechanism of gut microbe discerning and incorporating CNMs is still unknown, there are two possible ways: 1) Gut microbiota are always exposed to various types of particles originating endo- and exo-genously. With the frequent intake of nanomaterials by humans, gut microbes have evolved to be able to discern these "foreign" particles through the long-term domestication. For instance, the metabolic system of gut

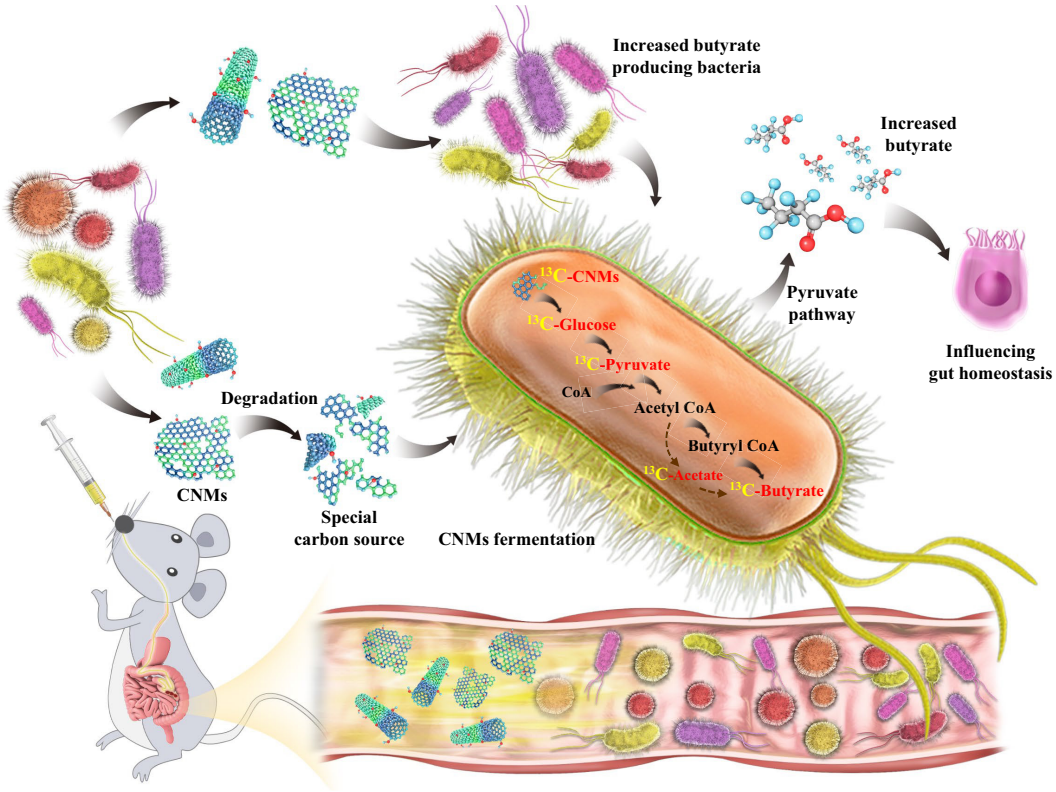

Fig. 6. Proposed new mechanisms to elucidate the biological processes and consequences of CNMs in the gut. When CNMs enter the gut lumen, the gut microbiota integrates CNMs as a special carbon source into the endogenous carbon flow through degradation and fermentation. In particular, the inorganic carbon from CNMs is incorporated into organic butyrate during the fermentation through the pyruvate pathway and relevant enzymes. In addition, CNMs induce a significant increase of butyrate-producing bacteria. These mechanisms contribute to the overproduction of butyrate that affects the function of intestinal stem cells and gut homeostasis.

microbiota has been domesticated to recognize exogenous nano coronaviruses or plastics (58, 59); 2) Gut microbiota are highly enriched for genes involved in carbon metabolism (49, 50), thus facilitating the host to extract calories from their normal diet or unconventional diet/source (CNMs).

In addition, as a special carbon source, CNMs facilitated the growth of butyrate-producing bacteria that dominated the production of butyrate from CNMs. It is worth noting that overproduction of butyrate induced by CNMs showed adverse consequences on the function of intestinal stem cells. These findings help to unravel the fermentation processes of nanomaterials in biological hosts and underscore the understanding pertinent to the field of nanosafety that engineered nanomaterials can not only directly interact with biological systems but also indirectly influence their host gut homeostasis through their fermented/transformed products. To be noticed, as gut microbiota consist of thousands of species of microbes, it is not possible to isolate pure enzymes in single bacterial or several bacterial strain from such a hugely complex system; further studies are warranted to reveal specific bacterial enzyme responsible for breaking down CNMs.

Materials and Methods

We include the detailed information of the materials and methods in *SI Appendix*, specifically preparation and characterization of SWCNTs and GO, experimental design for the degradation of SWCNTs and GO induced by gut bacteria, bacterial viability and number tests, HPLC analysis of SCFAs, verification of isotope butyrate derived from ^{13}C-labeled GO and test of pyruvate, calculation of ^{13}C atom number incorporation in products, activity and content of bacterial enzymes, animal experiments, haematology assay, histological assessment, Raman spectroscopy analysis of the degradation of SWCNTs and GO, matrix-assisted laser desorption ionization time-of-flight mass spectrometry analysis for the degradation of SWCNTs and GO, SDS polyacrylamide gel electrophoresis analysis for the degradation of SWCNTs and GO, effects of SIF on the degradation of SWCNTs and GO, gut microbiota analysis, flow cytometry analysis of intestinal stem cells, immunofluorescence of intestine, and isolation and culture of intestinal crypts and immunofluorescence as well as statistical analysis.

Data, Materials, and Software Availability. All the sequencing data are accessible at Sequence Read Archive (SRA) database with accession number PRJNA891872 (https://www.ncbi.nlm.nih.gov/sra/PRJNA891872) (60). All other data are included in the manuscript and/or *SI Appendix*.

ACKNOWLEDGMENTS. This work was supported by the National Key Research and Development Program of China (2021YFA1200900), the National Natural Science Foundation of China (32271460), the Major instrument project of National Natural Science Foundation of China (22027810), the Chinese Academy of Sciences Interdisciplinary Innovation Team, the Chinese Academy of Sciences Key Research Program for Frontier Sciences (QYZDJ-SS-SLH022), the Research and Development Project in Key Areas of Guangdong Province (2019B090917011), Chinese Academy of Medical Sciences Innovation Fund for Medical Sciences (2019-I2M-5-018), and the Strategic Priority Research Program of Chinese Academy of Sciences (XDB36000000).

Author affiliations: [a]Chinese Academy of Sciences Key Laboratory for Biomedical Effects of Nanomaterials and Nanosafety and Center for Excellence in Nanoscience, National Center for Nanoscience and Technology of China, Beijing 100190, China; [b]The GBA National Institute for Nanotechnology Innovation, Guangzhou 510700, Guangdong, China; [c]School of Nano Science and Technology, University of Chinese Academy of Sciences, Beijing 101400, China; [d]Chinese Academy of Sciences Key Laboratory for Biomedical Effects of Nanomaterials and Nanosafety, Institute of High Energy Physics, Beijing 100049, China; [e]State Key Laboratory of Environmental Chemistry and Ecotoxicology, Research Center for Eco-Environmental Sciences, Chinese Academy of Sciences, Beijing 100085, China; and [f]SCIEX China, Beijing 100020, China

1. E. Valsami-Jones, I. Lynch, How safe are nanomaterials? *Science* **350**, 388–389 (2015).
2. C. Wang *et al.*, Clinically approved carbon nanoparticles with oral administration for intestinal radioprotection via protecting the small intestinal crypt stem cells and maintaining the balance of intestinal flora. *Small* **16**, 1906915 (2020).
3. J. H. Ji, J. B. Kim, G. Lee, G. N. Bae, Nanomaterial release characteristics in a single-walled carbon nanotube manufacturing workplace. *J. Nanopart. Res.* **17**, 77 (2015).
4. H. Wang, W. Su, M. Tan, Endogenous fluorescence carbon dots derived from food items. *Innovation* **1**, 100009 (2020).
5. A. Barra *et al.*, Graphene derivatives in biopolymer-based composites for food packaging applications. *Nanomaterials* **10**, 2077 (2020).
6. X. Liu, M. Wang, S. Zhang, B. Pan, Application potential of carbon nanotubes in water treatment: A review. *J. Environ. Sci.* **25**, 1263–1280 (2013).
7. P. L. Yap *et al.*, Graphene-based sorbents for multipollutants removal in water: A review of recent progress. *Adv. Funct. Mater.* **31**, 2007356 (2021).
8. A. A. Koelmans *et al.*, Comparison of manufactured and black carbon nanoparticle concentrations in aquatic sediments. *Environ. Pollut.* **157**, 1110–1116 (2009).
9. J. Kolosnjaj-Tabi *et al.*, Anthropogenic carbon nanotubes found in the airways of parisian children. *EBioMedicine* **2**, 1697–1704 (2015).
10. M. Wu *et al.*, Case Report: Lung disease in World Trade Center responders exposed to dust and smoke: Carbon nanotubes found in the lungs of World Trade Center patients and dust samples. *Environ. Health. Perspect.* **118**, 499–504 (2010).
11. M. M. Dahm *et al.*, Exposure assessments for a cross-sectional epidemiologic study of US carbon nanotube and nanofiber workers. *Int. J. Hyg. Environ. Health* **221**, 429–440 (2018).
12. J. D. Beard *et al.*, Carbon nanotube and nanofiber exposure and sputum and blood biomarkers of early effect among U.S. workers. *Environ. Int.* **116**, 214–228 (2018).
13. B. Fadeel, K. Kostarelos, Grouping all carbon nanotubes into a single substance category is scientifically unjustified. *Nat. Nanotechnol.* **15**, 164 (2020).
14. Y. Tu *et al.*, Destructive extraction of phospholipids from Escherichia coli membranes by graphene nanosheets. *Nat. Nanotechnol.* **8**, 594–601 (2013).
15. X. Lu *et al.*, Long-term pulmonary exposure to multi-walled carbon nanotubes promotes breast cancer metastatic cascades. *Nat. Nanotechnol.* **14**, 719–727 (2019).
16. I. Lynch, Far-reaching effects from carbon nanotubes. *Nat. Nanotechnol.* **14**, 639–640 (2019).
17. G. Peng *et al.*, Graphene oxide elicits microbiome-dependent type 2 immune responses via the aryl hydrocarbon receptor. *Nat. Nanotechnol.* **18**, 42–48 (2023).
18. S. P. Mukherjee *et al.*, Graphene Oxide Elicits Membrane Lipid Changes and Neutrophil Extracellular Trap Formation. *Chem* **4**, 334–358 (2018).
19. M. G. Rooks, W. S. Garrett, Gut microbiota, metabolites and host immunity. *Nat. Rev. Immunol.* **16**, 341–352 (2016).
20. Y. Fan, O. Pedersen, Gut microbiota in human metabolic health and disease. *Nat. Rev. Microbiol.* **19**, 55–71 (2021).
21. X. J. Cui, L. Bao, X. Y. Wang, C. Y. Chen, The nano-intestine interaction: Understanding the location-oriented effects of engineered nanomaterials in the intestine. *Small* **16**, 1907665 (2020).
22. E. A. Mutlu, P. A. Engen, Particulate matter air pollution causes oxidant-mediated increase in gut permeability in mice. *Part. Fibre Toxicol.* **8**, 19 (2011).
23. A. Koh, F. De Vadder, P. Kovatcheva-Datchary, F. Backhed, From dietary fiber to host physiology: Short-chain fatty acids as key bacterial metabolites. *Cell* **165**, 1332–1345 (2016).
24. R. Kurapati *et al.*, Degradation of Single-layer and few-layer graphene by neutrophil myeloperoxidase. *Angew. Chem. Int. Ed.* **57**, 11722–11727 (2018).
25. B. L. Allen *et al.*, Biodegradation of single-walled carbon nanotubes through enzymatic catalysis. *Nano Lett.* **8**, 3899–3903 (2008).
26. V. E. Kagan *et al.*, Carbon nanotubes degraded by neutrophil myeloperoxidase induce less pulmonary inflammation. *Nat. Nanotechnol.* **5**, 354–359 (2010).
27. Y. Zhao, B. L. Allen, A. Star, Enzymatic degradation of multiwalled carbon nanotubes. *J. Phys. Chem. A* **115**, 9536–9544 (2011).
28. F. T. Andon *et al.*, Biodegradation of single-walled carbon nanotubes by eosinophil peroxidase. *Small* **9**, 2721–2729 (2013).
29. K. Lu, S. Dong, T. Xia, L. Mao, Kupffer cells degrade (14)C-labeled few-layer graphene to (14)CO_2 in liver through erythrophagocytosis. *ACS Nano* **15**, 396–409 (2020).
30. S. Yoshida *et al.*, A bacterium that degrades and assimilates poly(ethylene terephthalate). *Science* **351**, 1196–1199 (2016).
31. R. S. Chouhan *et al.*, Biotransformation of multi-walled carbon nanotubes mediated by nanomaterial resistant soil bacteria. *Chem. Eng. J.* **298**, 1–9 (2016).
32. L. W. Zhang, E. J. Petersen, M. Y. Habteselassie, L. Mao, Q. G. Huang, Degradation of multiwall carbon nanotubes by bacteria. *Environ. Pollut.* **181**, 335–339 (2013).
33. A. N. Parks, G. T. Chandler, K. T. Ho, R. M. Burgess, P. L. Ferguson, Environmental biodegradability of [(1)(4)C] single-walled carbon nanotubes by Trametes versicolor and natural microbial cultures found in New Bedford Harbor sediment and aerated wastewater treatment plant sludge. *Environ. Toxicol. Chem.* **34**, 247–251 (2015).
34. F. Candotto Carniel *et al.*, Graphene environmental biodegradation: Wood degrading and saprotrophic fungi oxidize few-layer graphene. *J. Hazard. Mater.* **414**, 125553 (2021).
35. X. J. Cui *et al.*, Crucial role of P2X7 receptor in regulating exocytosis of single-walled carbon nanotubes in macrophages. *Small* **12**, 5912–5912 (2016).
36. L. Chen *et al.*, Bioaccumulation and toxicity of ^{13}C-skeleton labeled graphene oxide in wheat. *Environ. Sci. Technol.* **51**, 10146–10153 (2017).
37. M. Afshari, Z. Abusara, N. Dehghani, N. Moazzen-Ahmadi, A. R. W. McKellar, Isotope effects in the infrared spectrum of the OCS dimer. *Chem. Phys. Lett.* **437**, 23–27 (2007).
38. M. Afshari, M. Dehghani, Z. Abusara, N. Moazzen-Ahmadi, A. R. W. McKellar, Infrared spectra of the polar isomer of the OCS dimer: ($^{16}O^{12}C^{32}S)_2$, ($^{16}O^{12}C^{34}S)_2$, and ($^{16}O^{13}C^{32}S)_2$. *Chem. Phys. Lett.* **442**, 212–216 (2007).
39. S. E. Pryde, S. H. Duncan, G. L. Hold, C. S. Stewart, H. J. Flint, The microbiology of butyrate formation in the human colon. *FEMS Microbiol Lett.* **217**, 133–139 (2002).
40. P. Louis *et al.*, Restricted distribution of the butyrate kinase pathway among butyrate-producing bacteria from the human colon. *J. Bacteriol.* **186**, 2099–2106 (2004).
41. M. T. Geng *et al.*, Structure, expression, and functional analysis of the hexokinase gene family in cassava. *Int. J. Mol. Sci.* **18**, 1041 (2017).
42. Y. Liu *et al.*, Galangin and pinocembrin from propolis ameliorate insulin resistance in HepG2 cells via regulating Akt/mTOR signaling. *Evidence-Based Complementary Altern Med.* **2018**, 1–10 (2018).
43. S. H. Duncan, A. Barcenilla, C. S. Stewart, S. E. Pryde, H. J. Flint, Acetate utilization and butyryl coenzyme A (CoA):Acetate-CoA transferase in butyrate-producing bacteria from the human large intestine. *Appl. Environ. Microbiol.* **68**, 5186–5190 (2002).
44. J. Hou *et al.*, Biodegradation of single-walled carbon nanotubes in macrophages through respiratory burst modulation. *Int. J. Mol. Sci.* **17**, 409 (2016).
45. J. Russier *et al.*, Oxidative biodegradation of single- and multi-walled carbon nanotubes. *Nanoscale* **3**, 893–896 (2011).
46. J. Goodrich *et al.*, Conducting a microbiome study. *Cell* **158**, 250–262 (2014).
47. R. E. Ley, P. J. Turnbaugh, K. Samuel, J. I. Gordon, Microbial ecology: Human gut microbes associated with obesity. *Nature* **444**, 1022–1023 (2006).
48. P. J. Turnbaugh *et al.*, An obesity-associated gut microbiome with increased capacity for energy harvest. *Nature* **444**, 1027–1031 (2006).
49. J. J. Qin *et al.*, A human gut microbial gene catalogue established by metagenomic sequencing. *Nature* **464**, 59–U70 (2010).
50. W. Wang *et al.*, Increased proportions of bifidobacterium and the lactobacillus group and loss of butyrate-producing bacteria in inflammatory bowel disease. *J. Clin. Microbiol.* **52**, 398–406 (2014).
51. G. E. Kaiko *et al.*, The colonic crypt protects stem cells from microbiota-derived metabolites. *Cell* **165**, 1708–1720 (2016).
52. H. J. Snippert, Colonic crypts: Safe haven from microbial products. *Cell* **165**, 1564–1566 (2016).
53. K. Kretzschmar, H. Clevers, Organoids: Modeling development and the stem cell niche in a dish. *Dev. Cell* **38**, 590–600 (2016).
54. J. Kumar, K. Rani, C. Datt, Molecular link between dietary fibre, gut microbiota and health. *Mol. Biol. Rep.* **47**, 6229–6237 (2020).
55. J. P. Segain *et al.*, Butyrate inhibits inflammatory responses through NFκB inhibition: Implications for Crohn's disease. *Gut* **47**, 397–403 (2000).
56. H. M. Hamer *et al.*, Review article: The role of butyrate on colonic function. *Aliment. Pharmacol. Ther.* **27**, 104–119 (2008).
57. M. S. Inan *et al.*, The luminal short-chain fatty acid butyrate modulates NF-kappa B activity in a human colonic epithelial cell line. *Gastroenterology* **118**, 724–734 (2000).
58. S. Donati Zeppa, D. Agostini, G. Piccoli, V. Stocchi, P. Sestili, Gut microbiota status in COVID-19: An unrecognized player? *Front. Cell. Infect. Microbiol.* **10**, 576551 (2020).
59. Z. Zhang *et al.*, Polyvinyl chloride degradation by a bacterium isolated from the gut of insect larvae. *Nat. Commun.* **13**, 5360 (2022).
60. X. J. Cui, The effect of *nanomaterials* on the *gut* microbiota. *Sequence Read Archive (SRA) database*. https://www.ncbi.nlm.nih.gov/sra/PRJNA891872. Accessed 20 October 2022.